A COUPLED OCEAN-ECOSYSTEM MODEL OF THE ROSS SEA. PART 1: INTERANNUAL VARIABILITY OF PRIMARY PRODUCTION AND PHYTOPLANKTON COMMUNITY STRUCTURE

Denise L. Worthen

Science Systems and Applications, Inc., Lanham, Maryland

Kevin R. Arrigo

Department of Geophysics, Stanford University, Stanford, California

Results from a high-resolution ocean-ecosystem model of the Ross Sea Antarctica for the period 1979-1998 are presented. The dominant surface species composition in the central shelf region of the model varies during the 1979-1998 period, with diatoms favored during 5 summers; the remaining summers were characterized by *P. antarctica*-dominance. Diatoms were favored in years with shallow (~10 m) mixed layer depths. Slower ice retreat, higher ice melt rates and weaker wind speeds favor shallow mixed layer depths in the model. Mean summer primary productivity is 10% higher in diatom years (0.96 g C m^{-2} d^{-1}) compared to *P. antarctica*-dominated years (0.80 g C m^{-2} d^{-1}). Average annual productivity in diatom years was found to be 98.8 g C m^{-2} yr^{-1} compared to 80.0 g C m^{-2} yr^{-1} in *P. antarctica*-dominated years. Productivity is higher in diatom years because of incomplete utilization of iron by diatoms, resulting in a weak, late *P. antarctica* bloom in these years. The model results indicate that if surface stratification were to increase in the central Ross Sea shelf region as a result of increasing anthropogenic CO_2, a significant shift in dominant species composition would occur. The model indicates that under such conditions, iron limitation on the central Ross Sea shelf would be reduced.

1. INTRODUCTION

Recently, *Arrigo et al.* [in press] reported on the use of a high resolution ocean-ecosystem model capable of simulating many of the observed properties of the Ross Sea ecosystem. The model contained two phytoplankton species representing *P. antarctica* and diatoms, a single grazer, detritus and the nutrients iron and nitrate. By invoking photoinhibition of *P. antarctica* in high irradiance and shallow mixed layers, the authors were able to simulate the observed species distribution, characterized by diatoms on the western shelf and *P. antarctica* in the central shelf. *Arrigo et al.* [in press] showed that under climatological forcing, mixed layer depth determined species composition in the model Ross Sea. Furthermore, iron was found to be critical in determining the annual productivity in the model. Annual productivity in the model was lowest in the *P. antarctica*-dominated central shelf due to iron limitation while the diatom-dominated western and eastern shelf regions had enhanced productivity associated with summer meltwater influx of iron into surface waters.

Interannual variations in wind speed and ice conditions affect three critical components identified in the climatological model: the spring iron concentration (derived from deep water sources), the summer mixed layer depth and the summer surface iron flux. The sensitivity of the modeled species composition and primary productivity to these variations must be evaluated in order to gauge the sensitivity of the modeled ecosystem to either short or long term climate perturbations. Such perturbations may include an increase in precipitation and intensified ocean surface stratification as a result of increasing anthropogenic CO_2 [Sarmiento et al., 1998]. Recent studies [Arrigo et al., 1999; Arrigo et al., in press] have suggested that increasing surface stratification could result in a shift in phytoplankton community composition from P. antarctica to diatoms. Such a taxonomic shift has implications for global biogeochemical models which assume that CO_2 draw-down is proportional to PO_4 removal [Sarmiento and Le Quere, 1996; Sarmiento et al., 1998]. In these models, a shift in the predominant community from P. antarctica to diatoms would decrease the CO_2 draw-down estimated from the C:P ratio by approximately 52% [Arrigo et al., 1999].

In order to evaluate the sensitivity of the Ross Sea coupled ocean-ecosystem model described by Arrigo et al. [in press] to interannual variation in environmental forcing, a 19 year integration from 1979-1998 was carried out. Described here are the variations in species composition and primary productivity within the central shelf region of the model in response to interannual variation in atmospheric and sea ice forcing.

2. THE MODEL

The ecosystem model used in this study contains two species of phytoplankton (P. antarctica and diatoms), a single zooplankton species, detritus and two nutrients (iron and nitrate). In the model, P. antarctica is shade-acclimated and photoinhibited at high light levels. Diatoms have a higher intrinsic growth rate, a lower iron affinity, a lower iron requirement and are adapted to high light levels (Table 1). Iron and nitrate, depleted from the surface layers during the summer growth season, are replenished with high concentration near-bottom waters by winter-time deep convective mixing. Aeolian-deposited iron incorporated into snow and ice is released into the ocean surface layer during spring and summer ice melt. Grazers are non-discriminating, with the prey capture rate and assimilation rate assumed equal for P. antarctica and diatoms. A complete description of the

TABLE 1. Model phytoplankton parameters

Description	Value
P. antarctica max. specific growth rate	0.59 d^{-1}
Diatom maximum specific growth rate	0.71 d^{-1}
P. antarctica photoadaptation parameter	30 $\mu Ein\ m^{-2}\ s^{-1}$
Diatom max. photoadaptation parameter	90 $\mu Ein\ m^{-2}\ s^{-1}$
P. antarctica half-saturation for Fe	0.01 nM
Diatom half-saturation for Fe	0.10 nM
P. antarctica photoinhibition threshold	100 $\mu Ein\ m^{-2}\ s^{-1}$

ecosystem model and it's response to climatological forcing can be found in Arrigo et al. [in press].

The ecosystem model is embedded into the Princeton Ocean Model (POM), a primitive equation ocean circulation model for a hydrostatic, incompressible and Boussinesq fluid [Blumberg and Mellor, 1987] with an embedded turbulence closure model [Mellor and Yamada, 1982]. It has a free surface and utilizes a terrain-following σ-coordinate system in the vertical and a curvilinear coordinate system in the horizontal. The model predicts the three dimensional fields of potential temperature, salinity, and velocity in response to surface and lateral boundary conditions of heat, salt, and momentum. A complete description of the model equations and numerical scheme can be found in Mellor [1996] and references therein.

2.1. Surface Fluxes

The specifications of surface fluxes applied to the POM model in this study are based on standard flux calculations and remotely sensed sea ice concentration. The specifications of surface fluxes in the present model were previously described by Markus [1999] using a mixed layer model of the Southern Ocean and are included here for completeness.

The surface flux of heat in W m^{-2}, defined positive for surface cooling, is

$$F_T = (1-A)\ Q_{ao} + AQ_{io} \qquad (1)$$

where A is the specified ice concentration, Q_{ao} is the flux of heat from ocean to atmosphere [Parkinson and Washington, 1979], and Q_{io} is the flux of heat from the ocean to the ice.

The heat flux from ocean to ice Q_{io} is given by

$$Q_{io} = K_i(T_0 - T_f) \qquad (2)$$

[Maykut and McPhee, 1995] where T_0 is the temperature of the first vertical grid point and $T_f = -0.0543S_0$ is

the freezing temperature at S_0, the salinity of the first vertical grid point. The coefficient K_i (W m^{-2} K^{-1}) depends on the friction velocity and is given by

$$K_i = \rho_w c_p c_h u_*$$ (3)

where ρ_w = 1026 kg m^{-3} is the density of seawater, c_p = 3990 J kg^{-1} K^{-1} is the heat capacity of seawater, c_h = 0.006 is Stanton number, and $u^* = |\tau|/\rho_w$ is the friction velocity calculated from the surface stress.

The surface stress τ for ice-covered regions is given by

$$\tau = (1-A)\tau_w + A\tau_i$$ (4)

where τ_w is the air-water stress and τ_i is the ice-water stress. The air-water stress is given by

$$\tau_w = \rho_w c_d |U_{10m}| U_{10m}$$ (5)

where c_d = 2.2×10^{-3} is the air-water drag coefficient, and U_{10m} is the 10 m wind vector. The ice-water stress τ_i is determined by the relative velocity between the ice and water. Since in the present model ice is not a prognostic variable, no ice velocities are available and a simplifying assumption must be employed. Here, the ice water stress τ_i is approximated by $r\tau_w$ [Tang, 1991]. For the present model r is set to a value of 1, representing a value midway between land fast ice (r =0) and freely drifting ice (r =2).

The 10 m wind fields used to calculate u^* give an average value of the parameter K_i in the Ross Sea between 60 and 300 W m^{-2} K^{-1} during the year. Values of K_i determined by the 10 m wind fields were found to generate large volumes of shelf water with salinity greater than 35 psu, primarily as a result of relatively weak heat flux at the ocean-ice interface. As a result, in the present model a constant value K_0 is added to the right hand side of Eq. 7; the value of K_0 used in the present model is 600 W m^{-2} K^{-1}. The total value of K_i used is well within the range of K_i values from the scientific literature which include 2 W m^{-2} K^{-1} [Willmott and Mysak, 1989], 300 W m^{-2} K^{-1} [Tang, 1991] and 1260 W m^{-2} K^{-1} [Häkkinen, 1987].

The heat flux from ice to atmosphere in Q_{ai} is

$$Q_{ai} = \frac{k_i k_s (T_f - T_a)}{k_i h_s + k_s h_i}$$ (6)

[Semtner, 1976] where T_a is the 2 m air temperature, k_s = 0.31 W m^{-2} K^{-1} and k_i = 2.04 W m^{-2} K^{-1} are the thermal conductivities of snow and ice, respectively, h_s is the thickness of snow, and h_i = 0.5 m is the specified ice thickness.

The net volumetric ice production W_o in m s^{-1}, positive for ice growth and negative for ice melt, is given by

$$W_o = (1-A) W_{ao} + A W_{io}$$ (7)

where the net basal melting (positive) or accumulation (negative) W_{io} in m s^{-1} is

$$W_{io} = \frac{Q_{io} - Q_{ai}}{L \rho_i}$$ (8)

and the open water freezing (positive) W_{ao} in m s^{-1} is

$$W_{ao} = \frac{Q_{ao}}{L \rho_i}$$ (9)

where L = 3.347×10^5 J kg^{-1} is the latent heat of fusion of seawater and ρ_i = 930 kg m^{-3} is the density of sea ice. The salinity flux at the surface of the ocean in psu m^{-1} s^{-1}, positive for surface freshening, is

$$F_s = (1-A)[PS_0 - W_{ao}(S_0 - S_{fi})] + A\frac{\rho_i}{\rho_w} W_{io}(S_0 - S_i)$$ (10)

where P = 0.35 m yr^{-1} is the specified precipitation rate distributed evenly through the year [Harder and Lemke, 1994], S_{fi} = 0.31S_0 is the salinity of frazil ice [Martin and Kaufmann, 1981] and S_i = 5 psu is the ice salinity [Eicken, 1998].

2.2. Initialization and Forcing

The model domain for this study encompasses the Ross Sea sector of the Southern Ocean extending from 135°E to 60°W and from 58°S to 78°S (Figure 1). The closed northern boundary was chosen to lie in a region of relatively zonal flow and the extent of the model domain was chosen to minimize the effect of lateral open boundaries on the region of interest. The southern boundary of the model in the region of the Ross Ice Shelf is closed. The horizontal grid spacing varies over the model domain, with highest resolution on the continental shelf of the Ross Sea, south of Cape Adare and west of 150°W. The model grid spacing on the Ross Sea shelf varies from a minimum of $\delta x \sim \delta y \sim 21$ km at the southern boundary to a maximum of $\delta x \sim \delta y \sim 31$ km near Cape Adare. Model grid spacing increases away from the Ross Sea shelf to maximum $\delta x \sim 180$ km and $\delta y \sim 100$ km at the northern boundary. The bottom topography for the model grid was interpolated from the TerrainBase5 data set (supplemented by the General Bathymetric Chart of the Oceans (GEBCO) data set). The minimum depth of
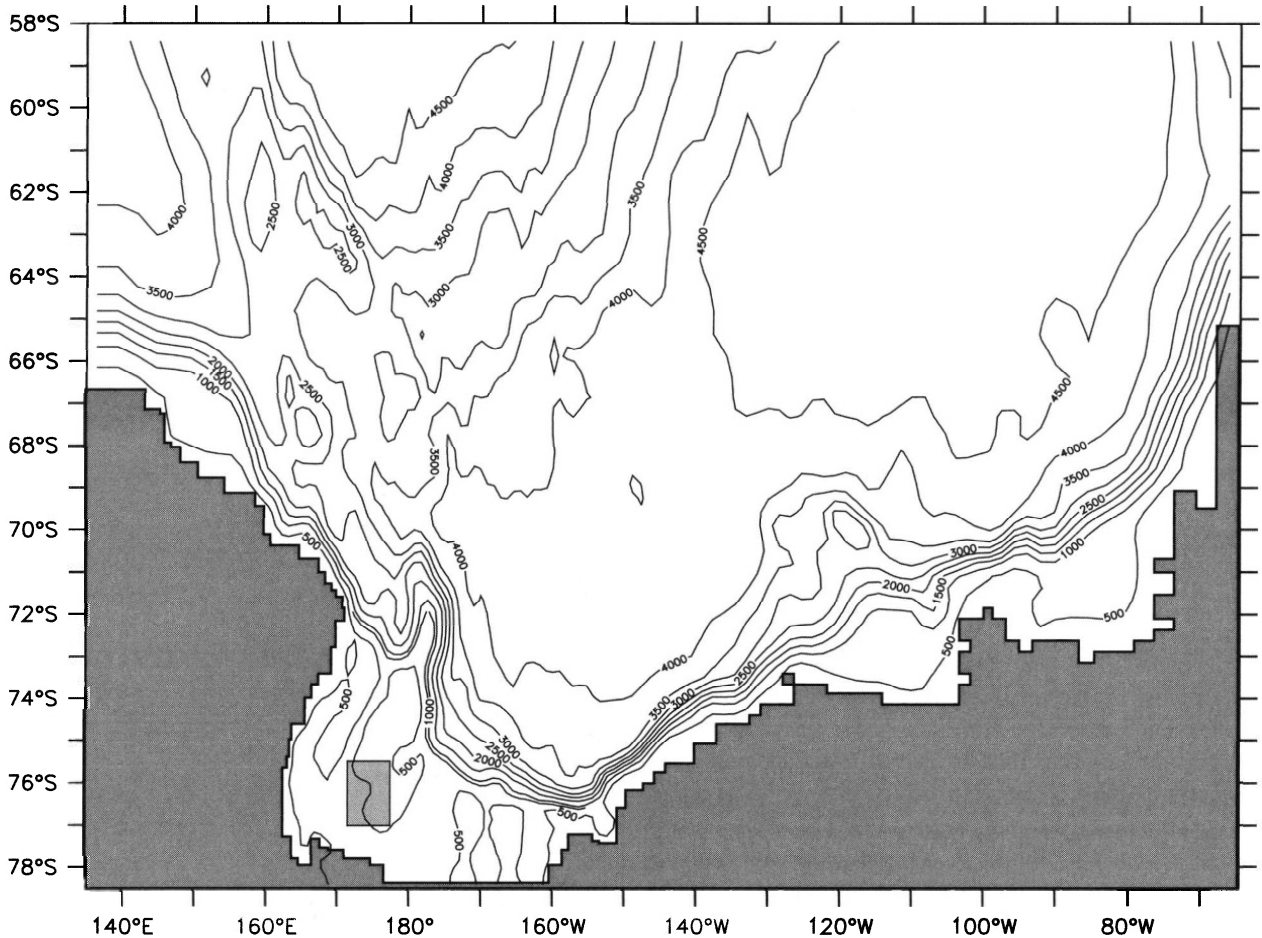
Fig. 1. The Ross Sea model domain. The 800 m isobath is highlighted. The region defined as the central Ross Sea shelf is indicated by the light gray box.

the model domain is approximately 50 m. The 23 σ-levels in the model are distributed smoothly in the vertical with an emphasis on resolution in the upper 200 m of the water column.

Atmospheric conditions required to force the model include total cloudiness, zonal and meridional winds at 10 m, sea level pressure, and specific humidity and air temperature at 2 m. The surface forcing fields were the daily mean products obtained from the National Centers for Environmental Prediction/National Center for Atmospheric Research Reanalysis Project [*Kalnay et al.*, 1996] for the period 1979-1998 provided by the NOAA-CIRES Climate Diagnostics Center. The daily average values were further averaged over 5 day periods to create a long term (1979-1998) mean 5 day surface forcing data set. Similarly, the sea ice concentrations for the period 1979-1998, calculated using the NASA Team algorithm [*Cavalieri et al.*, 1984; *Gloersen and Cavalieri*, 1986;

Cavalieri et al., 1992], were averaged into a long term 5 day mean data set. Monthly mean snow cover for 1979-1998 [*Markus and Cavalieri*, 1998] were averaged to form a long term monthly mean snow coverage. A second set of 5 day mean atmospheric and sea ice data and monthly mean snow data was created in similar fashion for each individual year in the 1979-1998 period.

The results discussed here are from a 19 year run beginning 1 July 1979 and continuing through to 30 June 1998. The model was initialized from the ocean-ecosystem model state at the end of a 70 year integration under climatological 5 day mean forcing [*Arrigo et al.*, in press]. During each year of integration in the 19 year run, daily averages of model fields were saved on the 7th, 14th, 21st, and 28th calendar day of each month. For the purposes of model results presented here, the central Ross Sea shelf is defined as 172°E to 177°E and from 77°S to 75.5°S. This 24,000 km² region typically encompasses

both the Ross Sea polynya and the peak summer bloom within the model and represents approximately 6% of the total shelf (depth <800 m) area. For each year of model integration, the daily mean model fields were area-averaged within the defined central Ross Sea shelf region.

3. RESULTS AND DISCUSSION

3.1. Variation of Surface Forcing

The mean 10 m wind speed in the central Ross Sea region undergoes significant variation during the 19 year model integration (Figure 2a). From the start of the model integration in 1979 through 1986 the mean wind speed in the model is 3.7 m s^{-1}. During this period, minimum summer (mid-December) wind speeds are <2.0 m s^{-1} and peak autumn (March) wind speeds reach 5.0 m s^{-1}. Between January 1987 and the end of March 1992 the mean wind speed is 6.3 m s^{-1}, a 70% increase over the previous mean value. The seasonal range of wind speeds is smaller in this period, from a summer minimum of about 5.0 m s^{-1} to a autumn maximum of about 8.0 m s^{-1}. After March 1992, the mean wind speed decreases again to 4.5 m s^{-1}, with a seasonal range of 3.0 m s^{-1} to about 7.0 m s^{-1}. A similar temporal variation in wind speed during the 19 year integration, though with a smaller variation in range,
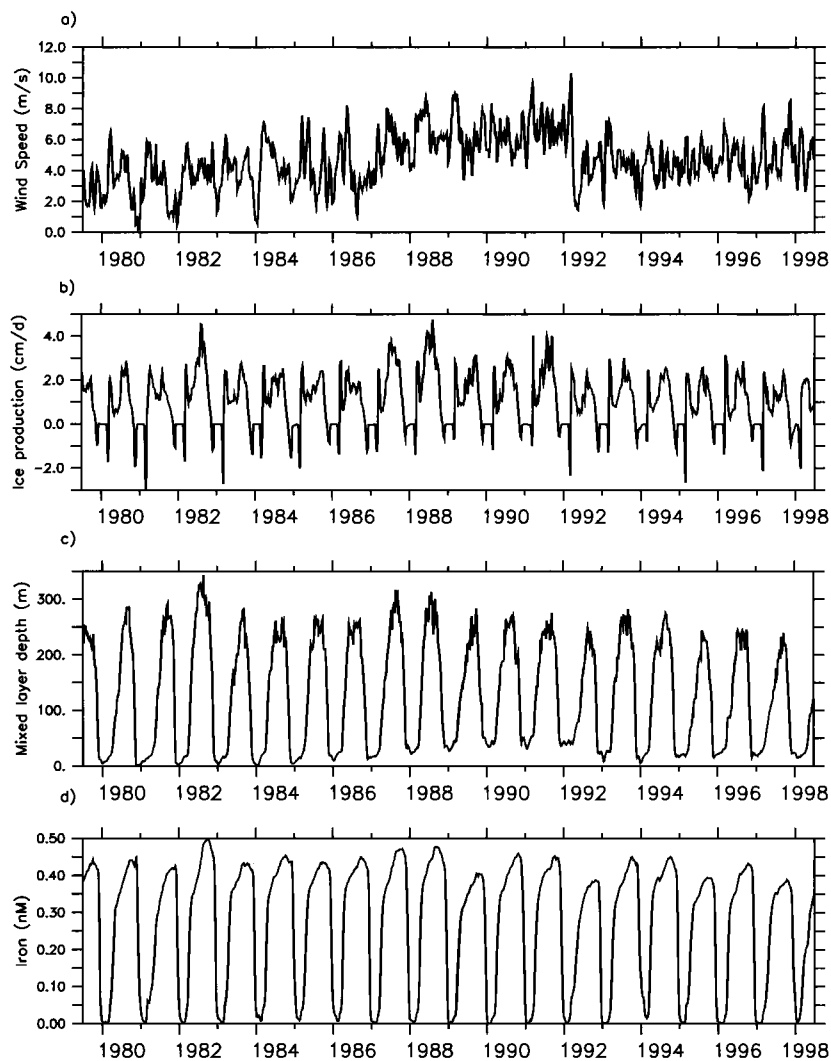

Fig. 2. The a) 10-m wind speed (m s^{-1}) b) ice production (cm d^{-1}), c) mixed layer depth (m) and d) upper 20 m iron concentration (nM) in the central Ross Sea region during the 19 year model integration.

is also seen on the western and eastern shelf of the model (not shown). The temporal variation in wind speed over the Ross Sea shelf illustrates one of the shortcomings of using a relatively coarse (2.5° × 2.5°) resolution global model to specify atmospheric forcing in a region of notoriously sparse data sources.

Regional mean ice production in the model (Figure 2b) generally peaks in early August at about 25 mm d^{-1}, though ice production rates in excess of 40 mm d^{-1} occur in 1982, 1988, and 1991. Because ice conditions in the model are specified using observed satellite data, the variation in wind speed between 1987 and 1992 discussed above is not reflected in a similar temporal trend in ice production in these years. Summer ice melt typically begins in mid-November and peaks at the end of November at about –10 mm d^{-1}. The spring melt rates in 1980-1984 are significantly higher than normal, with an average value in these years of –14 mm d^{-1}. A second ice melt period occurs in late February as the fall freeze-up begins. This additional ice melt is due to a lag between the model predicted surface temperatures which are still above freezing at this time and the specification of ice concentration derived from satellite observations. Autumn ice melt during this period is generally slightly stronger than in summer, with an average value of about –12 mm d^{-1}.

Mixed layer depths in the central Ross Sea region of the model vary from as deep as 340 m to less than 10 m (Figure 2c) during the model integration. The deepest mixed layers are reached in late August to mid-September, a time when the water column is only marginally stable and brine rejection during sea ice formation leads to deep convective mixing. Winter mixed layers are deepest in years with high rates of sea ice production regardless of the wind regime. As ice production wanes in late October and summer ice melt begins, mixed layers begin to shoal; by the end of November mixed layer depths are near 20 m. Summer mixed layer depths are deepest during the period of strongest winds, reaching more than 40 m deep at the end of December 1990. Absorption of solar radiation in shallow mixed layers leads to warmer surface temperatures and enhanced ice melt (Figure 2b) compared to years with deeper mixed layers.

The highest iron concentrations in the central Ross Sea are reached in mid to late winter (Figure 2d) as deep convective mixing replenishes the iron-depleted surface water with deep and bottom water [Arrigo et al., in press]. Years with higher winter ice production rates and deeper winter mixed layer depths have higher spring iron concentrations. The 19 year mean upper 20 m iron concentration in late winter is 0.44 nM, with values as high as 0.50 nM in 1982 and as low as 0.39 nM in 1992.

3.2. Variation of Species Composition

The modeled interannual variability of surface species composition in the central Ross Sea shelf region in the 1979-1998 period is shown in Figure 3. During the first six years of the model integration, the summer (DJF) seasons were dominated by December diatom blooms (Figure 3a). These diatom blooms began as early as mid-November and peaked in mid-December with chlorophyll a (Chl a) values greater than 10 mg m^{-3} (Figure 3b), reaching almost 20 mg m^{-3} in both 1981-1982 and 1984-1985. Beginning in 1986, the species composition in the model switched to P. antarctica-dominance, continuing in that mode except for the single 1993-1994 season when diatoms became the dominant species in early January. Surface Chl a concentrations were lower in P. antarctica-dominated years, with peak values usually less than 8 mg Chl a m^{-3}.

The range of mean surface Chl a in the model during the 19 year integration is within the satellite observed surface Chl a in this region. In the model, the peak surface Chl a values range from about 7.3 mg m^{-3} to almost 20 mg m^{-3}. Satellite observations from CZCS, OCTS and SeaWiFS show that the mean Chl a in the region of the central Ross Sea shelf ranges from about 3.0 mg m^{-3} in mid-December 1996 to more than 16.0 mg m^{-3} in early January 1978. The model tends to slightly overestimate the surface Chl a values, especially in years when the satellite observations report low Chl a values. The compressed range of the model surface Chl a values compared to the satellite record is most likely due to the limitations imposed by using 5 day mean atmospheric data to force the model. In particular, the fractional cloudiness fields in the model tend to remain between 0.4 and 0.6 resulting in surface irradiance values which tend to compress the dynamic range of the model surface Chl a values.

A comparison between model output and in situ data is complicated by the differing spatial and temporal scales of the model output and data collected from the field. Surface Chl a values measured in situ between 16 December 1996 and 8 January 1997 were as high as 7.0 mg m^{-3} [Arrigo et al., 1999] (at a single station), with a mean value of more than 5.0 mg m^{-3} in the central Ross Sea shelf region. In comparison, the peak surface Chl a value in the central Ross Sea region of the model during the 1996-1997 season was 13.6 mg m^{-3}; the regional mean value reaches a peak of 8.5 mg m^{-3}. The species composition measured in situ was predominantly P. antarctica, in agreement with the model species composition which was more than 85% P. antarctica during December 1996.
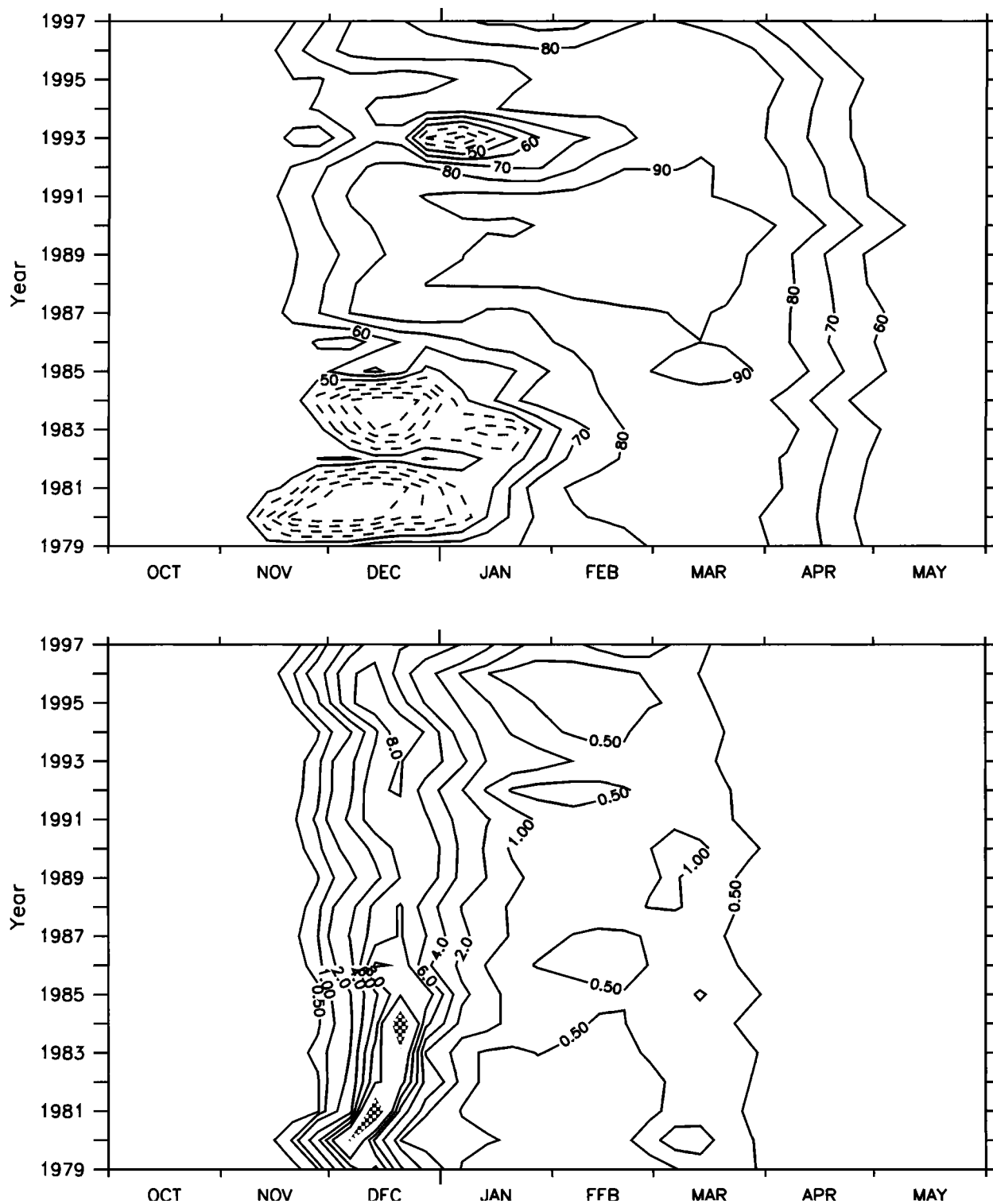
Fig. 3. The surface a) species composition (%) and b) biomass (mg Chl a m^{-3}) in the central Ross Sea shelf region during the model integration. Species composition is defined as the percent of the total biomass represented by each species. In a) the contour interval is 10%; solid lines refer to *P. antarctica* and dashed lines to diatoms. In b) the contour interval is 2 mg Chl a m^{-3} between 0 and 10 mg Chl a m^{-3}; the stippled regions indicate values greater than 15 mg Chl a m^{-3}.

As shown by *Arrigo et al.* [in press], species composition in the model is determined by mixed layer depth. Deep mixed layers favor *P. antarctica*, as the shade-acclimated *P. antarctica* out-compete diatoms in low irradiance waters; shallow mixed layers favor diatoms due to photoinhibition of *P. antarctica* at high irradiance levels. Diatoms tend to dominate within the first years of the model integration when summer wind speeds are lowest (Figure 2a) and mixed layers most shallow (Figure 2c). Mid-November wind speeds are approximately 50% lower for the model years when diatoms dominate the surface waters of the central Ross Sea (1980-81, 1981-82, 1983-84, 1984-85 and 1993-1994) compared to *P. antarctica* years (2.3 m s⁻¹ vs. 5.2 m s⁻¹). The resulting mixed layer depths throughout the summer season are significantly lower in diatom years (Figure 4), averaging 9.8 m for diatom years compared to 25 m in *P. antarctica*-dominated years.

Shallow mixed layers and diatom-dominance are determined by ice conditions which include later ice retreat and stronger ice melt. Summer ice melt and mixed layer depth are coupled through the absorption of solar radiation, which warms the surface waters of shallow mixed layers, leading to enhanced ice melt. Since sea ice concentration in the model is specified from satellite observations, higher ice melt rates (and warmer, shallower mixed layers) result when ice persists later in the austral spring. In the model, diatom-dominated years have an average ice concentration in mid-November (0.51) that is approximately 10% higher than in *P. antarctica* years (0.46). The central Ross Sea shelf region becomes ice-free (defined as a mean ice concentration ≤0.20) an average of 5 days later in diatom years (julian day 335) compared to *P. antarctica* years (julian day 330). Warmer surface temperatures in the shallow mixed layers of diatom years result in mid-November ice melt which is approximately 3 times higher (−03.8 mm d⁻¹ vs. −1.3 mm d⁻¹) than in *P. antarctica*-dominated years.

3.3. Variation of Primary Productivity

Total integrated productivity in the model increases rapidly in a one month period, from an average of <0.1 g

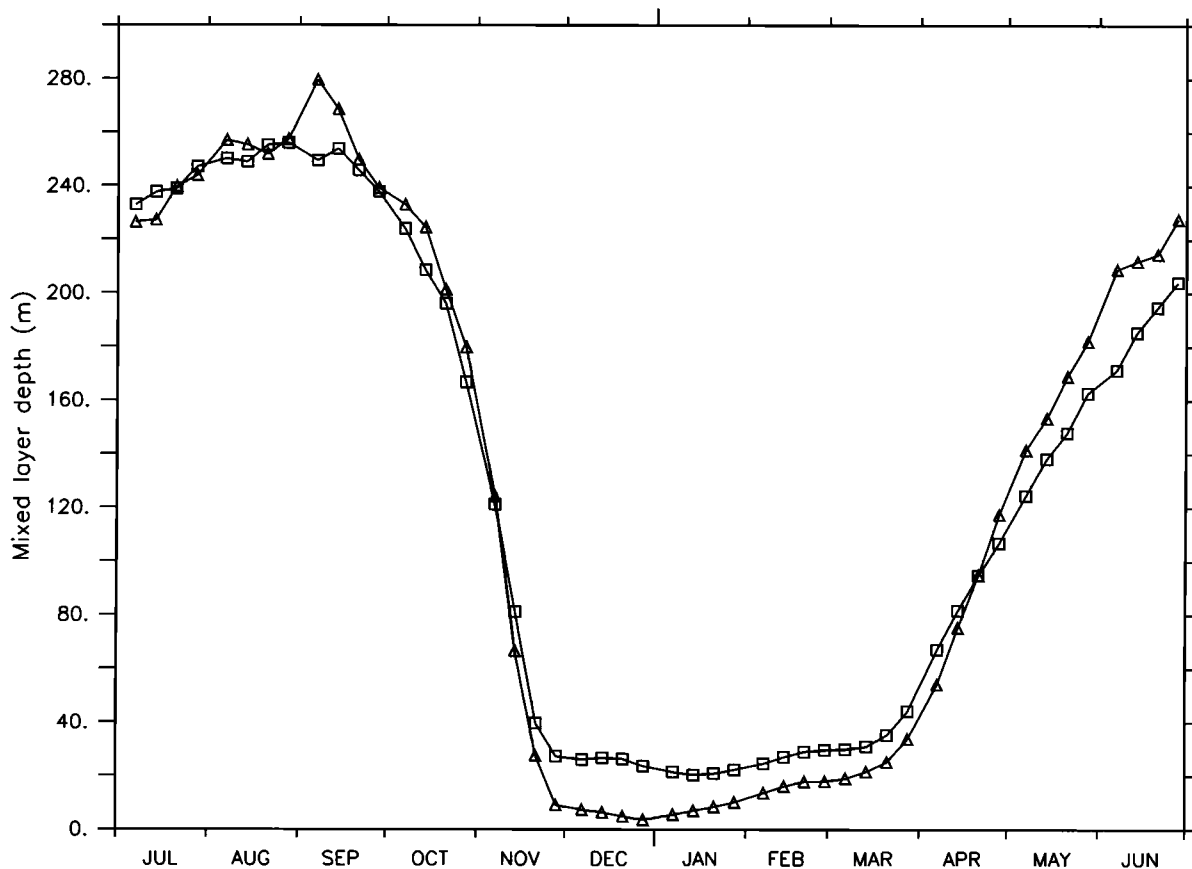Fig. 4. The average mixed layer depth (m) in years dominated by diatoms (△) and *P. antarctica* (☐).

C m^{-2} d^{-1} in mid-November to 2.0 g C m^{-2} d^{-1} by mid-December. The subsequent decline in productivity takes place over a much longer period, with a mean productivity value of 0.37 g C m^{-2} d^{-1} as late as mid-February. The yearly productivity peak during the 19 year integration ranges from a high of about 2.9 g C m^{-2} d^{-1} in December 1981 to about 1.7 g C m^{-2} d^{-1} in December 1993 (Figure 5). Mid-February productivity ranges from 0.59 g C m^{-2} d^{-1} in February 1998 to 0.25 g C m^{-2} d^{-1} in February 1997.

The variation in total integrated productivity shown in Figure 5 is not directly related to the species composition at the surface. While diatoms dominate at the model surface in years with shallow mixed layers, P. antarctica are favored at depths below the mixed layer where irradiance levels are lower and photoinhibition is unimportant. In diatom-dominated years, P. antarctica biomass peaks at about 2.0 mg Chl a m^{-3} at depths between 10 and 20 m (Figure 6). Thus, even at the time of peak surface diatom biomass, about 27% of the integrated daily productivity is attributable to P. antarctica (Figure 6a). Conversely, in P. antarctica-dominated years, diatoms reach 2 mg Chl a m^{-3} in the near surface waters (Figure 6b), significantly less than the ~8 mg Chl a m^{-3} seen in diatom years, but still high enough to contribute roughly 20% to the peak integrated productivity (Figure 7b).

The variation in peak productivity in the model is primarily related to interannual variations in mixed layer
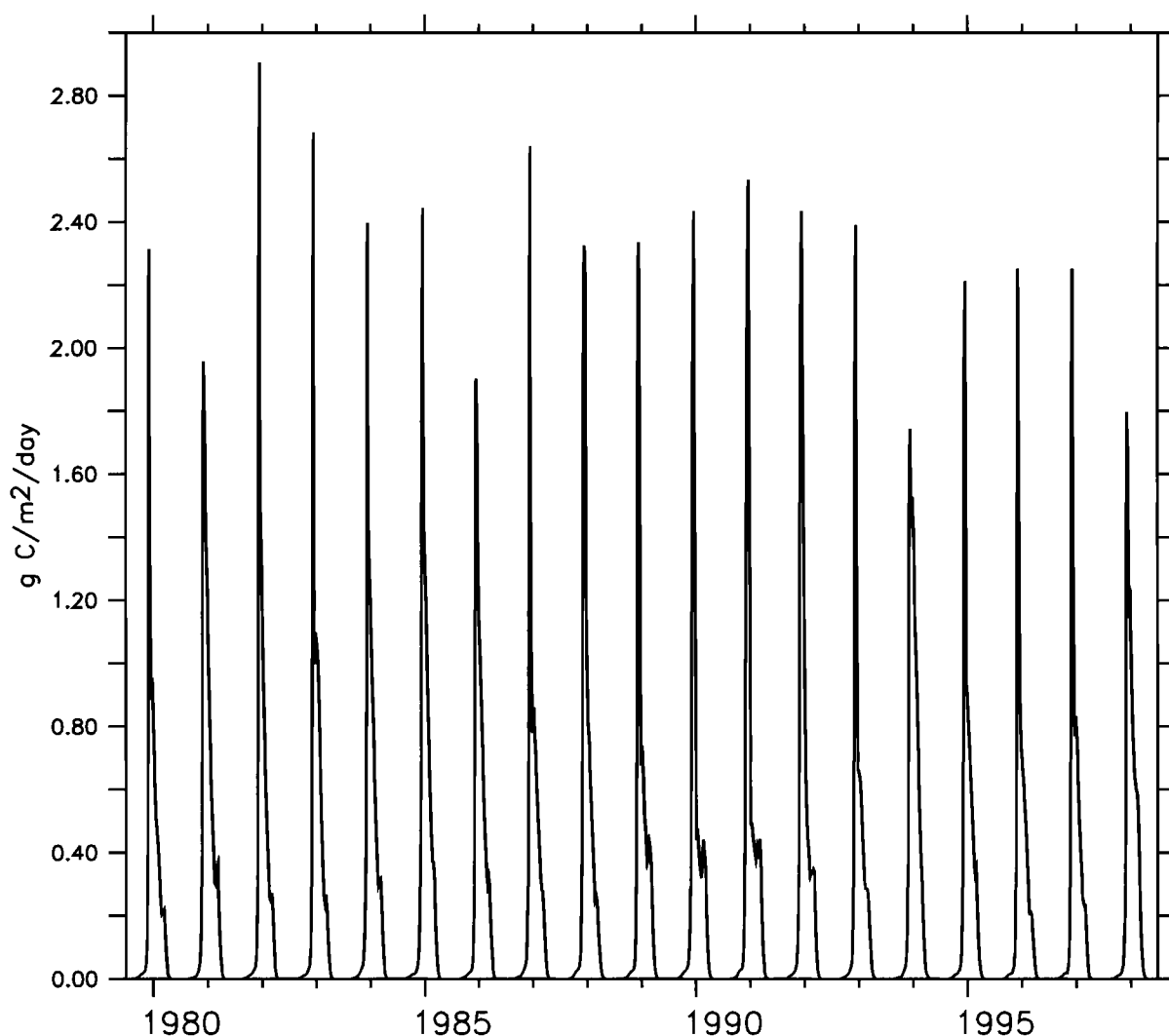

Fig. 5. The daily total (P. antarctica + diatoms) integrated production (g C m^{-2} d^{-1}) during the model integration.

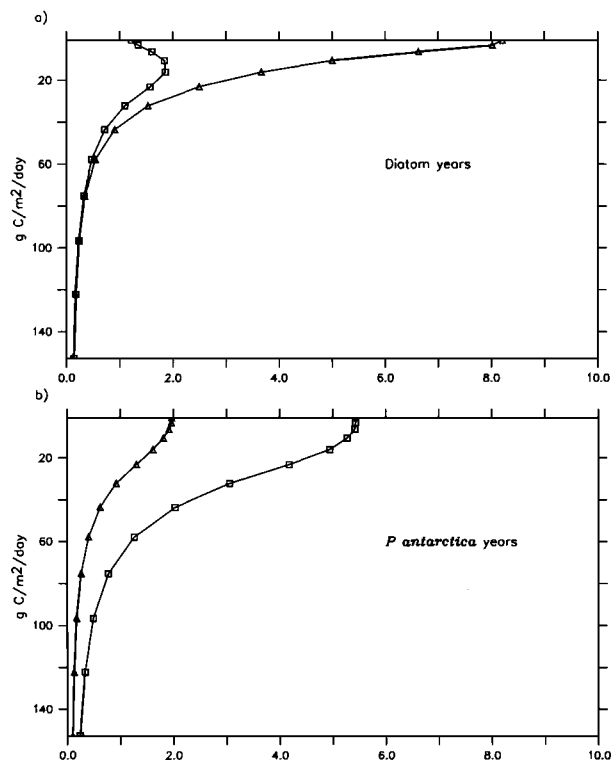Fig. 6. The profile of diatom (Δ) and *P. antarctica* ($\square$) biomass (mg Chl a m^{-3}) in mid-December in years dominated by a) diatoms and b) *P. antarctica*.

development and surface iron concentration in late November and early December. For example, in both 1980-1981 and 1981-1982, diatoms dominate at the surface and the peak productivities are 2.0 g C m^{-2} d^{-1} and 2.9 g C m^{-2} d^{-1}, respectively (Figure 5). In both these years, strong ice melt and very light summer wind speeds produce very shallow ($\leq$10 m) mixed layers (Figure 2). Photoinhibition of *P. antarctica* is particularly strong, resulting in extremely low *P. antarctica* biomass within the mixed layer; *P. antarctica* contributes less than 0.40 g C m^{-2} d^{-1} (12%) to the peak total integrated productivity in these years. The variation in peak productivity between years is determined by the diatom productivity; in 1980-1981, the shallow mixed layer develops in mid-November, about 2 weeks earlier than in 1981-1982 and much earlier than the time of peak summer irradiance. Diatoms in 1980-1981 become iron limited by early December, resulting in a much lower peak productivity in this year.

In both 1985-1986 and 1986-1987, *P. antarctica* dominates at the surface and the peak productivities in these years are 1.9 g C m^{-2} d^{-1} and 2.6 g C m^{-2} d^{-1}, respective-

ly (Figure 5). In both years, relatively strong 10 m wind speeds and weak ice melt result in mixed layer depths greater than ~15 m through mid-December (Figure 2). In 1985-1986, however, the mixed layer shoals briefly after mid-December in response to weaker winds beforedeepening again after mid-January. The *P. antarctica* bloom is moderated by the shoaling mixed layer, resulting photoinhibition and a peak *P. antarctica* productivity of less than 1.40 g C m^{-2} d^{-1}. More importantly however, the peak diatom productivity in 1985-1986 occurs about a week after the peak *P. antarctica* productivity, during the period when the mixed layer shoals. This offset in *P. antarctica* and diatom peak productivity results in a lower productivity maximum, though one which extends over a slightly longer period.

3.4. Regulation of Primary Productivity

The mean summer daily productivity during the 19 year model integration was 0.88 g C m^{-2} d^{-1}, with a range from a low of 0.71 g C m^{-2} d^{-1} in 1996-1997 to more than 1.0 g C m^{-2} d^{-1} in 1984-1985 and 1993-1994. The annual productivity ranged from a low of 78 g C m^{-2} yr^{-1} in
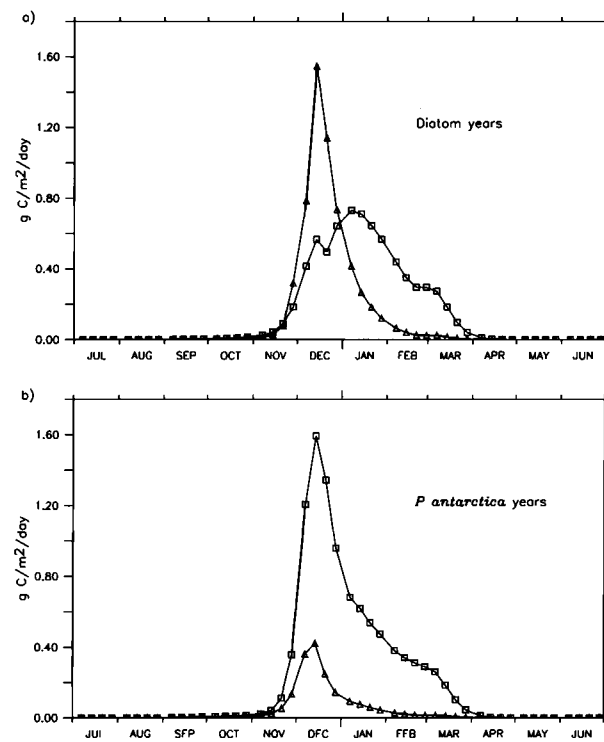

Fig. 7. The daily integrated productivity (g C m^{-2} d^{-1}) of diatoms (Δ) and *P. antarctica* ($\square$) in years dominated by a) diatoms and b) *P. antarctica*.

1992-1993 to a high of more than 104 g C m^{-2} yr^{-1} in 1993-1994, with a 19 year mean value of 92 g C m^{-2} yr^{-1}. In five of the 19 years, annual productivity was more than 100 g C m^{-2} yr^{-1}. The mean summer daily productivity was 10% higher in diatom-dominated years (0.96 g C m^{-2} yr^{-1}) than in *P. antarctica*-dominated years (0.85 g C m^{-2} yr^{-1}), reflecting the longer bloom in diatom years caused by an increase in *P. antarctica* productivity from early January through mid-February (Figure 7). This increase in late summer productivity resulted in annual production in diatom years (98.8 g C m^{-2} yr^{-1}) which was also 10% greater than in *P. antarctica*-dominated years (89.0 g C m^{-2} yr^{-1}).

The higher average daily and annual productivity in diatom years is a consequence of a shallow mixed layer, which itself is the result of slower ice retreat, greater ice melt, and lower wind speed. Since aeolian deposited iron is released into the surface layer of the model during ice melt [*Arrigo et al.*, in press], the slower ice retreat and higher ice melt rate also result in a November iron concentration that is about 0.07 nM higher at the surface in diatom years than in *P. antarctica*-dominated years. However, as surface iron drops below about 0.10 nM, the lower iron affinity of diatoms (K_s=0.10 nM) begins to limit their growth rate while the growth rate of *P. antarctica*, with a higher iron affinity (K_s=0.01 nM), is not limited by the depleted iron stock. Coupled with decreasing irradiance levels and increasing mixed layer depths (Figure 4) after mid-December, *P. antarctica* undergo a mild January bloom, yielding higher average summer productivity and annual production in diatom years. The central Ross Sea region finally becomes iron limited in mid-February in diatom-dominated years compared to early January in *P. antarctica*-dominated years (Figure 8).

4. CONCLUSIONS

The coupled ocean-ecosystem model of the Ross Sea described here illustrates that variations in atmospheric forcing and sea ice conditions alter both the species com-
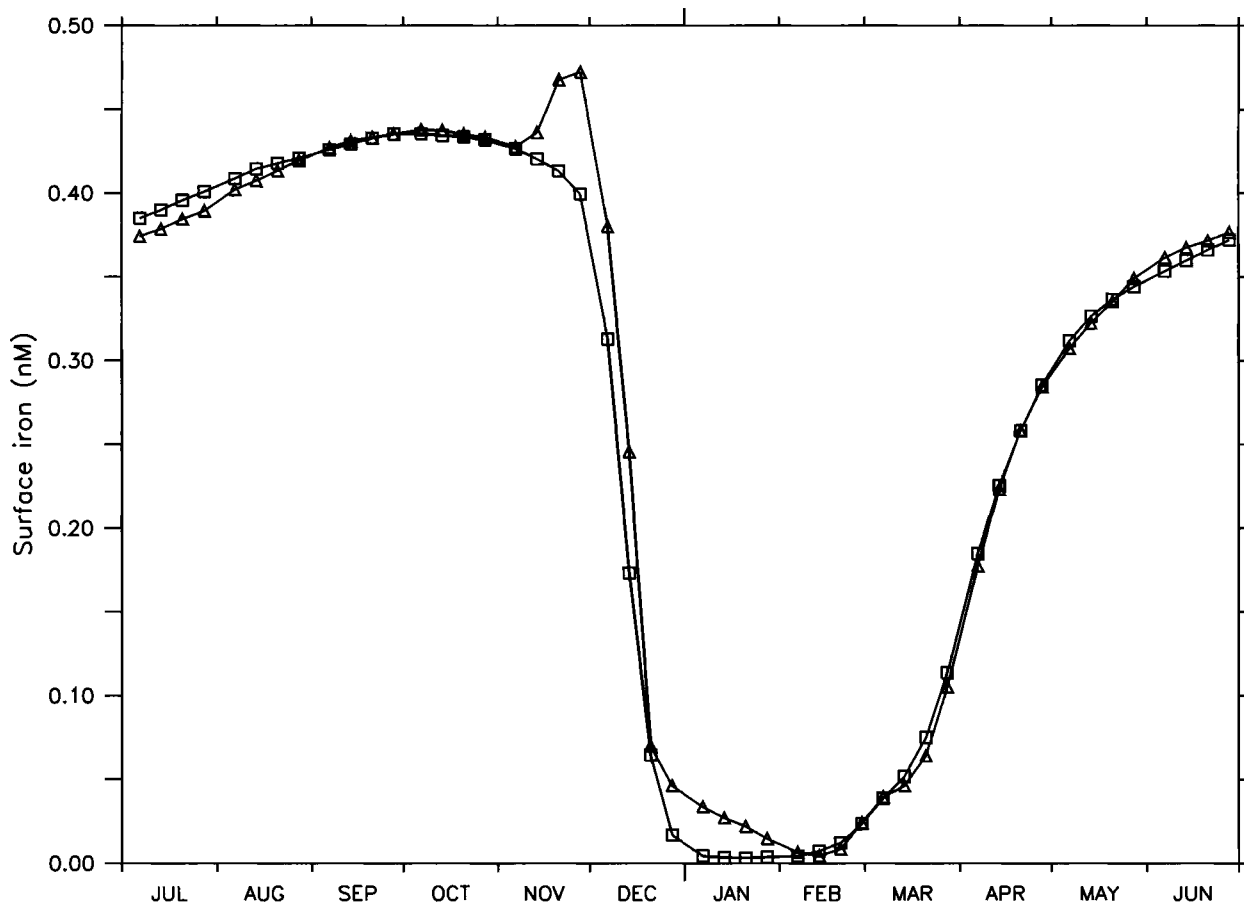

Fig. 8. The average surface iron concentration (nM) in years dominated by a) diatoms (△) and b) *P. antarctica* (□).

position as well as the annual primary productivity of the central Ross Sea. During the model integration period 1979-1998, diatoms were favored during five summers. Shallow mixed layer depths, the result of relatively high ice concentration, high ice melt and low wind speeds, favored diatoms in these years. Peak primary productivity rates were comparable in diatom and *P. antarctica* years. *P. antarctica* provides approximately one-third of the integrated productivity in diatom years while diatoms provide about one-fifth of the integrated productivity in *P. antarctica* years. Mean summer daily productivity in the central Ross Sea is 10% higher in diatom years because of low iron utilization by diatoms. Diatoms blooming early in this region do not deplete the surface iron, allowing for a late *P. antarctica* bloom to extend the productive period into mid-January. In diatom years, the annual productivity on the central Ross Sea is increased by approximately 10% by this secondary *P. antarctica* bloom.

The increase in productivity in years when diatoms dominate the central Ross Sea shelf is roughly comparable to that seen in the climatological model when comparing the diatom-dominated western and eastern shelves to the central Ross Sea [*Arrigo et al.*, in press]. In contrast to the western and eastern shelf regions where continual high rates of ice melt lead to summer surface iron concentrations in excess of 1.2 nM, summer iron concentrations in the central Ross Sea are primarily limited to the iron available at the start of summer growth season. This iron is derived from deep and bottom sources during the preceding winter and is not replenished during summer in the central Ross Sea because of the limited amount of ice melt which occurs in this region. *P. antarctica*, which are favored in the central Ross Sea in when deep mixed layers are present, have a relatively high iron requirement and rapidly deplete the surface iron. Both the climatological model and the interannual model support the thesis that productivity in the central Ross Sea is iron limited in years when *P. antarctica* dominates at the surface.

The interannual model results suggest that the central Ross Sea is not constrained to either *P. antarctica*-dominance or iron limitation. Given the correct set of atmospheric forcing and sea ice conditions, mixed layer depths within the central Ross Sea can be shallow enough to support an mid-December diatom bloom; in these years surface iron is sufficient to support an additional, albeit small, *P. antarctica* bloom in early January. The interannual model results also suggest that under increasing anthropogenic CO_2 levels, stronger surface stratification would produce a species shift in the central Ross Sea shelf. Such a shift would be accompanied by higher productivity rates as iron limitation in this region is reduced.

REFERENCES

Arrigo, K. R., D. H. Robinson, D. L. Worthen, R. B. Dunbar, G. R. DiTullio, M. L. Van Woert, and M. P. Lizotte, Phytoplankton community structure and the draw-down of nutrients and CO_2 in the Southern Ocean, *Science, 283*, 365-367, 1999.

Arrigo, K. R., G. R. DiTullio, R. B. Dunbar, M. P. Lizotte, D. H. Robinson, M. L. Van Woert, and D. L. Worthen, Phytoplankton taxonomic variability and nutrient utilization and primary productivity in the Ross Sea, *J. Geophys. Res., 105*, 8827-8846, 2000.

Arrigo, K. R., D. L. Worthen, and D. H. Robinson, A coupled ocean-ecosystem model of the Ross Sea. Part 2: Iron regulation of phytoplankton taxonomic variability and primary production, *J. Geophys. Res.*, in press.

Blumberg, A. F., and G. L. Mellor, A description of a three-dimensional coastal ocean circulation model, in *Three Dimensional Coastal Ocean Models, Coastal Estuarine Sci.*, vol. 4, edited by N. S. Heaps, pp. 1-16, AGU, Washington, D.C, 1987.

Cavalieri, D. J, P. Gloersen, and W. J. Campbell, Determination of sea ice parameters with the NIMBUS 7 scanning multichannel microwave radiometer, *J. Geophys. Res., 89*, 5355-5369, 1984.

Cavalieri, D. J. et al., NASA sea ice validation program for the DMSP SSM/I: Final report, *NASA Tech. Memo*, 104559, 126 pp, 1992.

Eicken, H., Deriving modes and rates of ice growth in the Weddell Sea from microstructural, salinity and stable-isotope data, in *Antarctic Sea Ice Physical Processes, Interactions and Variability*, edited by M.O. Jeffries, AGU, Washington, D.C., *Ant. Res. Ser. 74*, 89-122, 1998.

Gloersen, P., and D. J. Cavalieri, Reduction of weather effects in the calculation of sea ice concentration from microwave radiances *J. Geophys. Res., 91*, 3913-3919, 1986.

Häkkinen, S., A coupled dynamic-thermodynamic model of an ice-ocean system in the marginal ice zone, *J. Geophys. Res., 92*, 9469-9478, 1987.

Harder, M., and P. Lemke, Modeling the extent of sea ice ridging in the Weddell Sea, in *The Polar Oceans and Their Role in Shaping the Global Environment, The Nansen Centennial Volume*, edited by O.M. Johannessen, R.D. Muench and J. E. Overland, AGU, Washington, D.C., *Geophys. Monogr. Ser., 85*, 187-197, 1994.

Kalnay, E., et al., The NCEP/NCAR 40-year reanalysis project, *Am. Meteor. Soc., 77*, 437-471, 1996.

Markus, T., and D. J. Cavalieri, Snow depth distribution over sea ice in the Southern Ocean from satellite passive microwave data, in *Antarctic Sea Ice Physical Processes, Interactions, and Variability*, edited by M.O. Jeffries, AGU, Washington, D.C., *Ant. Res. Ser, 74*, 19-39, 1998.

Markus, T., Results from an ECMWF-SSM/I forced mixed layer model of the Southern Ocean, *J. Geophys. Res., 104*, 15603-15620, 1999.

Martin, S. and P. Kaufmann, A field and laboratory study of wave damping by grease ice, *J. Glaciol., 27*, 283-314, 1981.

Maykut, G. A., and M. G. McPhee, Solar heating of the Arctic mixed layer, *J. Geophys. Res.*, *100*, 24691-24703, 1995.

Mellor, G. L., and T. Yamada, Development of a turbulence closure model for geophysical fluid problems, *Rev. Geophys*, *20*, 851-875, 1982.

Mellor, G. L., User's guide for a three-dimensional, primitive equation, numerical ocean model, Program in *Atmos. and Ocean. Sci. Rep.*, 40 pp., Princeton Univ., Princeton, N. J, 1996.

Parkinson, C. L., and W. M. Washington, A large-scale numerical model of sea ice, *J. Geophys. Res.*, *84*, 311-337, 1979.

Sarmiento, J. L, and C. Le Quere, Ocean carbon dioxide uptake in a model of century-scale global warming, *Science*, *393*, 1346-1350, 1996.

Sarmiento, J. L., T. M. C. Hughes, R. J. Stouffer, and S. Manabe, Simulated response of the ocean carbon cycle to anthropogenic carbon warming, *Nature*, *393*, 245-249, 1998.

Semtner, A. J., Jr., A model for the thermodynamic growth of sea ice in numerical investigations of climate, *J. Phys. Oceanogr.*, *6*, 370-389, 1976.

Tang, C. L., A two-dimensional thermodynamic model for sea ice advance and retreat in the Newfoundland marginal ice zone, *J. Geophys. Res.*, *96*, 4723-4737, 1991.

Willmott, A. J., and L. A. Mysak, A simple steady state coupled ice-ocean model, with application to the Greenland-Norwegian Sea, *J. Phys. Oceanogr.*, *19*, 501-518, 1989.

Denise L. Worthen, Science Systems and Applications, Inc, 10210 Greenbelt Road, Suite 600 Lanham, MD 20706.

Kevin R. Arrigo, Department of Geophysics, Stanford University, Stanford, CA 94305-2215.